Anomalous Absorption of Very High-Intensity Laser Pulses Propagating through Moderately Dense Plasma

J. C. Adam, A. Héron, S. Guérin, G. Laval, P. Mora, and B. Quesnel
Centre de Physique Théorique (UPR14 du CNRS), Ecole Polytechnique, 91128 Palaiseau Cedex, France
(Received 3 October 1996)

The results of a systematic study of the propagation of very high-intensity laser pulses through slabs of plasma of several tens of microns are presented. One-dimensional and two-dimensional electron parametric instabilities are evidenced. They lead to a rapid longitudinal and transverse heating, and to filamentary structures which progressively merge. The heating results in highly energetic electrons with energy of several tens of MeV. Correlatively, a strong attenuation rate of the electromagnetic wave is observed. [S0031-9007(97)03413-3]

PACS numbers: 52.40.Nk, 52.35.Mw, 52.60.+h, 52.65.Cc

As a result of recent progress in optical processing, lasers reaching petawatt power are becoming available yielding intensities ranging from 10^{17} to 10^{20} W/cm^2 for which electrons relativistic effects become significant. The interaction of such laser beams with moderately underdense to slightly overdense plasma is of particular interest in the "fast ignitor" context [1] and is expected to display new physical phenomena [2–17].

In this Letter we study the propagation of large intensity picosecond laser pulses ($10^{18} < I < 10^{19}$ W/cm^2) through plasma slabs of thickness $60\lambda_0$ and electron density n ranging from $0.5n_c$ to $1.5n_c$. Here λ_0 is the laser wavelength and n_c is the critical density associated with the laser frequency ω_0, $n_c = m_e\varepsilon_0\omega_0^2/e^2$. Our important results are the following: (i) Even though transverse variations are allowed, the one-dimensional (1D) strongly coupled relativistic stimulated Raman scattering (RSRS) initially develops as predicted in Ref. [14] and heats electrons in the longitudinal direction; (ii) shortly after two-dimensional (2D) RSRS [18,19] leads to transverse heating and filamentary structures which in a nonlinear stage progressively merge; (iii) the strong absorption (ranging from 50% to 90% in our simulations) results in electrons of energy up to tens of MeV and in a large attenuation rate of the electromagnetic wave.

We use 2D particle-in-cell simulations, with either linear or circular polarization. The algorithm used is similar to the one of Ref. [20] with improvements as described in Ref. [21]. In most cases we restrict the present discussion for simplicity to the case of fixed ions. Other simulations have shown however that the essential features described in this paper are also seen in the more realistic cases of beams propagating through a plasma with mobile ions. Most simulations deal with an incident plane wave. However, we also discuss briefly simulations with Gaussian pulses with a full width at half maximum varying from $2\lambda_0$ to $10\lambda_0$, where λ_0 is the laser wavelength, which show essentially the excitation of the same instabilities. Except otherwise specified, simulations are performed with a simulation box of $100\lambda_0$ in the x (laser) direction and $37\lambda_0$ in the y (transverse) direction. The size of the mesh is about $0.05\lambda_0$ and there are typically ten particles per cell in the plasma slab, which corresponds to a total of about 9×10^6 particles. The length of the vacuum region in front of the plasma slab is $24\lambda_0$. The initial temperature is $T_e = 1$ keV. In all that follows we note $A_0 = p_0/m_e c$ the normalized quiver velocity in vacuum ($A_0 = 1$ corresponds to $I = 2.6 \times 10^{18}$ W/cm^2 for a circularly polarized wave and a wavelength of 1 μm).

Electron parametric instabilities in the relativistic domain have been extensively studied in 1D in [14] and extended to 2D in [18,19]. The 1D instability is the result of the coupling of four waves: the incident electromagnetic wave, a plasma wave and two (Stokes and anti-Stokes) electromagnetic scattered waves. The 2D instability further involves coupling of harmonics [18,19]. Figure 1 is a plot of the theoretical 1D growth rates [14] as a function of the plasma wave number k normalized to the vacuum laser wave number $k_0 = 2\pi/\lambda_0$, for A_0 ranging from 0.4 to 1.732 and $n/n_c = 0.5$. Note that the predicted growth rates are very high (reaching $0.4\omega_0$ for $A_0 = 1.73$). This implies that the linear regime can be observed only for a short time in the simulations, or for a slowly rising laser amplitude. Note also that the strongly coupled RSRS is effective even when $n > 0.25n_c^*$, where n_c^* is the

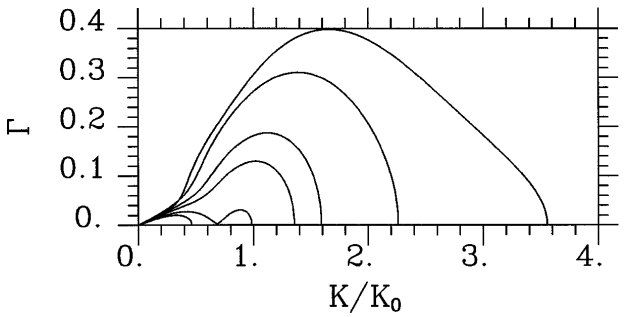

FIG. 1. Theoretical growth rate as a function of the wave number normalized to the vacuum wave number for $A_0 = 0.4$, 0.45, 0.55, 0.65, 1.0, and 1.732. The density is $n = 0.5n_c$.

relativistically corrected critical density, $n_c^* = \gamma n_c$ [with $\gamma = (1 + A_0^2)^{1/2}$].

The heating and absorption that we observe in the simulations are similar for linear or circular polarization. However, as the theoretical results concerning the electron parametric instabilities have been derived only for circular polarized light, most of the identification work has been done in this framework. Moreover in this case a signature of the onset of the instability is the development of electrostatic waves. The electrostatic part of the field is easily obtained in the simulations by solving the Poisson equation. The mode $k_y = 0$ of the electrostatic field is shown in Fig. 2 for a simulation with $n/n_c = 0.5$ and a normalized laser pulse amplitude rising linearly from 0 to $A_{\max} = 1.732$ with a (rather long) rise time $t_{\text{rise}} = 310\omega_0^{-1}$, followed by a plateau (ω_0^{-1} corresponds approximately to 0.5 fs for a 1 μm laser wavelength). Time $t = 0$ corresponds to the laser pulse reaching the edge of the plasma slab, defined by $k_0 x_{\text{edge}} \approx 150$. Figure 2(a) shows the structure of the electrostatic field at $t = 130\omega_0^{-1}$, when the value of the laser amplitude at x_{edge} is $A_{\text{edge}} = 0.74$. The weak modulation which is observed for $165 < k_0 x < 200$ is a weak residual $2\omega_0$ modulation superimposed to the charge separation field induced by the ponderomotive force (for a linear polarization this modulation is far stronger). On the other hand the perturbation which appears for $150 < k_0 x < 165$ can be attributed to the instability. Figure 2(b) shows the same field $20\omega_0^{-1}$ later ($A_{\text{edge}} = 0.85$). The development of a large perturbation at the edge of the slab of plasma with a value of $k \sim 1.1k_0$, close to a wave number corresponding to the theoretical maximum growth rate for the current value of the amplitude $A_0 \sim 0.65$ slightly inside the plasma, is clearly visible. The amplitude of the perturbation increases by a factor of 25–50 between the two considered times which corresponds to an averaged growth rate of $(0.16–0.20)\omega_0$ comparable with the theoretical growth rate for $A_0 = 0.6–0.7$.

Let us now discuss the initial heating mechanism in the longitudinal (forward) direction. The identification process is easy at a moderate intensity. Figure 3 represents the contour plots of the electron distribution function in the phase space (x, p_x) at time $t = 325\omega_0^{-1}$ for a simulation performed with $n/n_c = 0.5$, $A_{\max} = 0.35$, and $t_{\text{rise}} = 100\omega_0^{-1}$. Note the data have been integrated in the y direction. The picture shows the existence of phase space vortices which yields numerous fast particles mainly in the forward direction with values of p_x of the order of 2.5, reaching 4 later on. Note that the elliptical structure centered in the vicinity of $x = 310k_0^{-1}$ is a hole in phase with no particles in it. Later on, diffusion occurs filling the full phase space. In the case of Fig. 3 the phase velocities of the initially excited waves are far too large compared to the thermal velocities to invoke a resonant mechanism between plasma waves and particles, at least initially. For higher intensities, however, unstable modes with slower phase velocities can also be involved, so that the heating process becomes a mixture of trapping and stochastic heating.

Up to now we have considered only the development of the longitudinal ($k_y = 0$) perturbations. Sidescattering instabilities ($k_y \neq 0$) have a slightly smaller growth rate than the longitudinal ones [19], but develop almost simultaneously leading to a strong heating in the y direction. This is the fundamental new feature of 2D simulations compared with the 1D case. In the simulation of Fig. 2 transverse perturbations appear as soon as $t = 150\omega_0^{-1}$. Figure 4 shows contour plots of $|E_x(x, k_y)|$ in the (x, k_y) space (the Fourier transform is taken only in the y direction). The parameters are exactly those of Fig. 2(b). One can see that a broad spectrum has already developed with wave numbers extending up to $k_y = 1.5k_0$. The mode $k_y = 0$ [corresponding to Fig. 2(b)] is still dominant at this early time (its amplitude is 0.1 in the same unit as A_0); however,

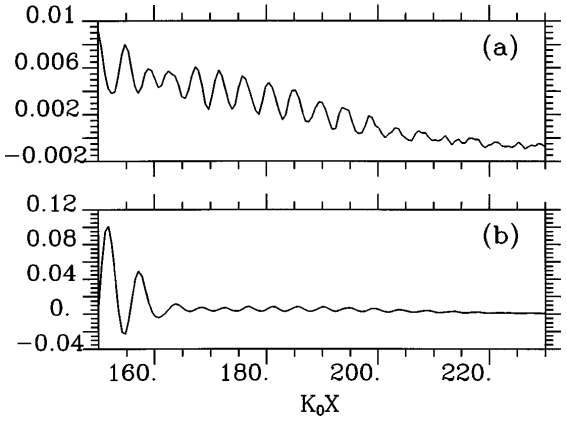

FIG. 2. Spatial structure of the mode $k_y = 0$ of electrostatic field in an underdense plasma, $n/n_c = 0.5$, as a function of x for (a) $t = 130\omega_0^{-1}$, $A_{\text{edge}} = 0.74$, and (b) time $150\omega_0^{-1}$, $A_{\text{edge}} = 0.85$. Note the change of scale between the two graphs.

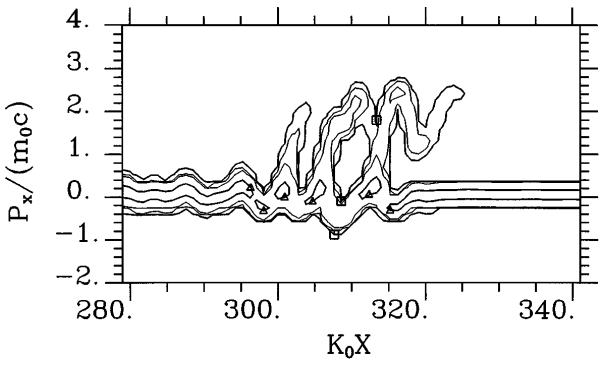

FIG. 3. Contour plots of the electron distribution function in the phase space, (x, p_x) at time $t = 325\omega_0^{-1}$ for a simulation performed with $n/n_c = 0.5$, $A_{\max} = 0.35$, and $t_{\text{rise}} = 100\omega_0^{-1}$. Time corresponds to the beginning of the nonlinear phase of development of the instability.

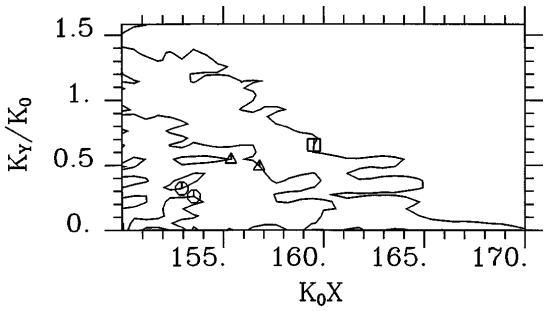

FIG. 4. Contour plots of $|E_x(x, k_y)|$ for the same parameters as Fig. 2(b). The contours correspond to isovalues of $|E_x(x, k_y)|$ in units of A_0 [0.003 (□), 0.01 (△), 0.03 (○)].

modes with amplitude above 0.01 can be observed up to $k_y = 0.8k_0$.

After this initial phase the nonlinear structure of the 2D perturbations becomes filamentary. At $t = 150\omega_0^{-1}$ about 20 filaments can be counted corresponding to an average wavelength of $1.9\lambda_0$. The number of filaments decreases rapidly and at $t = 450\omega_0^{-1}$, for which $A_{\text{edge}} = A_{\text{max}} = 1.732$, there are only six of them, as shown in Fig. 5. Their coalescence continues then more slowly and at $t = 1050\omega_0^{-1}$ only two remain. The maximum value of the Poynting vector within a filament is approximately twice A_0^2. The heating which takes place in the filaments generates highly energetic particles with a relativistic factor up to 40 as shown in Fig. 6 where the distribution of the relativistic factor γ as a function of x at $t = 450\omega_0^{-1}$ is plotted. It is also visible that a significant fraction of the particles has a value of γ larger than 10 in the region of penetration of the electromagnetic wave (up to $x = 350k_0^{-1}$). Some are even penetrating ahead of the front of propagation of the laser light. Though they are preferentially accelerated in the x direction, a significant transverse heating also occurs. The accelerated electrons generate strong electric currents in the axial direction, which, together with return currents, give rise to a quasistatic magnetic field in the 150 MG range. This magnetic field could be responsible for the merging of the filaments, as suggested in Ref. [16].

As stated at the beginning of this Letter an important feature in this regime of laser plasma interaction is the attenuation of the laser energy. During the propagation of the laser front in the plasma slab, the backscattered rate is of the order of 5%, with a characteristic frequency of approximately $0.5\omega_0$, in agreement with the theoretical predictions. Note that a significant part of the backscattered light corresponds to $k_y \neq 0$. This backscattering is due to the electron parametric instabilities discussed above. In the asymptotic state, i.e., well after the front of propagation has crossed the whole slab, the instabilities become less efficient in backscattering the energy, the corresponding electrostatic component being strongly Landau damped by hot electrons. As a result the energy is essentially absorbed or transmitted. The flux of energy of the electromagnetic wave normalized to the incident flux of energy as a function of space is plotted in Fig. 7 in the asymptotic state for three different simulations with $A_0 = 1.732$. The importance of the absorption is clearly visible as well as the low level of backscattering. The solid line corresponds to the case that has just been discussed ($n/n_c = 0.5$). The transmission coefficient is approximately 35% and the reflection is essentially zero.

The dotted and the dashed lines in Fig. 7 correspond to $n/n_c = 1.5$, i.e., to the regime of induced transparency [12,17], with fixed and mobile ions, respectively. In these two cases reflection is slightly more important than for $n/n_c = 0.5$ especially for the case with fixed ions where it reaches 5% due to the sharp discontinuity at the boundary of the slab. The transmission is also much weaker, about 7.5%. For the same parameters 1D simulations [17] exhibit much higher transmission rates. This clearly demonstrates the importance of transverse effects on the rate of absorption. In the present overdense 2D simulations, one observes on a very short time scale an initial forward

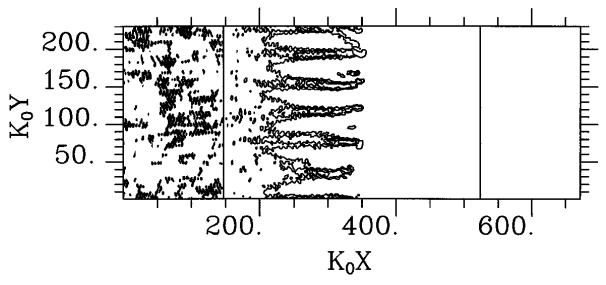

FIG. 5. Contour plots of the flux of the Poynting vector in the x direction as a function of space for the simulation of Fig. 2(b), at a later time, $t = 450\omega_0^{-1}$, for which $A_{\text{edge}} = A_{\text{max}} = 1.732$.

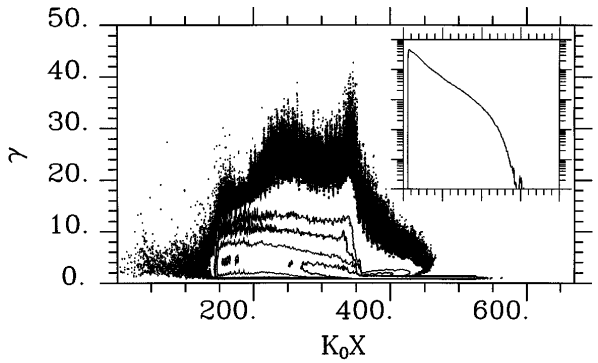

FIG. 6. Contour plots of the distribution function of γ for the parameters of Fig. 5. The contour plots are for isovalues of 5×10^4, 10^3, 500, 200, 100, and 20 in number of particles per cell in the (x, γ) space. The value of 5×10^4 corresponds to the bulk of the distribution function and 20 to the last isovalue. Below 20 the black part corresponds to a plot of individual "particles" (not numerous enough to define contour plots). The inset is a sample semilog plot of the normalized distribution function, averaged between $k_0x = 325$ and $k_0x = 350$. The vertical scale covers 5 decades (ranging from 10^{-6} to 10^{-1}) and the horizontal scale extends up to $\gamma = 40$.

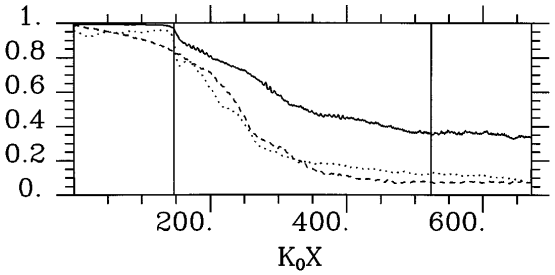

FIG. 7. Flux of electromagnetic energy in the x direction and normalized to the incident energy, as a function of space. The two vertical solid lines represent the initial edge of the plasma slab. The amplitude parameter is $A_{\max} = 1.732$. The solid line corresponds to $n/n_c = 0.5$. The dotted line corresponds to $n/n_c = 1.5$ and fixed ions; the dashed line corresponds to the same density and mobile ions, with $m_i/m_e = 1836$. Time is $1450\omega_0^{-1}$ for the solid line and $1850\omega_0^{-1}$ for the dotted and dashed lines. The energy flux is averaged over one laser period.

heating with $p_x \sim 20$ with an almost simultaneous and similar transverse heating. The situation is more complicated than in the case of an underdense plasma because here there exists a discontinuity of the index of refraction at the front of propagation due to the relativistic effects [12,17]. As a result a large ambipolar field is present in the region penetrated by the electromagnetic wave. This ambipolar field is difficult to distinguish from the field generated by the instability. Nevertheless, in the transverse direction the spectrum of plasma waves is similar to the underdense case, which suggests that the transverse heating is related to the same instability.

The simulations show that large growth rates occur for modes with $k_y \sim k_0$ for a wide class of parameters which implies that transverse effects play a major role as soon as the system is no longer purely 1D. Runs with a simulation box limited to $2.2\lambda_0$ in the transverse direction continue to exhibit the transverse instability and the associated heating. This also remains true for simulations with focalized beams. Even for beams having a very narrow initial width $(2.2\lambda_0)$, one can still observe the development of the instability (i.e., the appearance of plasma waves with $k_y \sim k_0$), and heating of the plasma before self-focusing takes place.

In summary the systematic study of ultraintense laser beam propagating through long slabs of underdense to moderately overdense plasma has confirmed the existence of the strong 1D and 2D relativistic parametric instabilities studied in [14,17–19]. The instabilities readily lead to an important absorption of the incident pulse and to the generation of highly energetic particles.

The computations were performed using IDRIS, the CNRS central computing facility.

[1] M. Tabak *et al.,* Phys. Plasmas **1**, 1826 (1994).
[2] A. I. Akhiezer and R. V. Polovin, Zh. Eksp. Teor. Fiz. **30**, 915 (1956) [Sov. Phys. JETP **2**, 696 (1958)].
[3] P. Kaw and J. Dawson, Phys. Fluids **13**, 472 (1970).
[4] C. Max, J. Arons, and A. B. Langdon, Phys. Rev. Lett. **33**, 209 (1974).
[5] A. B. Langdon and B. Lasinski, Phys. Rev. Lett. **34**, 934 (1975).
[6] D. W. Forslund *et al.,* Phys. Rev. Lett. **54**, 558 (1985).
[7] W. B. Mori *et al.,* in *Laser Interaction and Related Plasma Phenomena,* edited by H. Hora and G. Miley (Plenum Press, New York, 1986), Vol. 7, p. 767.
[8] W. B. Mori *et al.,* Phys. Rev. Lett. **60**, 1298 (1988).
[9] T. M. Antonsen, Jr. and P. Mora, Phys. Fluids B **5**, 1440 (1993).
[10] S. C. Wilks *et al.,* Phys. Rev. Lett. **69**, 1383 (1992); S. C. Wilks, Phys. Fluids B **5**, 2603 (1993); S. Wilks *et al.,* Phys. Rev. Lett. **73**, 2994 (1994).
[11] G. A. Askar'yan *et al.,* Pis'ma Zh. Eksp. Teor. Fiz. **60**, 240 (1994) [JETP Lett. **60**, 251 (1994)].
[12] E. Lefebvre and G. Bonnaud, Phys. Rev. Lett. **74**, 2002 (1995).
[13] P. Monot *et al.,* Phys. Rev. Lett. **74**, 2953 (1995).
[14] S. Guérin *et al.,* Phys. Plasmas **2**, 2807 (1995).
[15] J. C. Adam *et al.,* J. Phys. (Paris), Colloq., Suppl. IV, **5**, C6-1 (1995).
[16] A. Pukhov and J. Meyer-ter-Vehn, Phys. Rev. Lett. **76**, 3975 (1996).
[17] S. Guérin *et al.,* Phys. Plasmas **3**, 2693 (1996).
[18] A. S. Sakharov and V. I. Kirsanov, Plasma Phys. Rep. **21**, 632 (1995).
[19] B. Quesnel *et al.,* Phys. Rev. Lett. **78**, 2132 (1997).
[20] A. B. Langdon and B. Lasinski, in *Methods of Computational Physics* (Academic Press, New York, 1976), Vol. 9, p. 327.
[21] J. C. Adam *et al.,* J. Comput. Phys. **47**, 2 (1982).